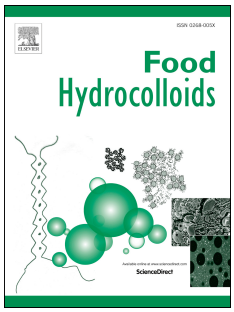

Food-protecting films based on soy protein isolate and natural deep eutectic solvents: Antimicrobial and antioxidant properties

Pablo A. Mercadal, Matias L. Picchio, Agustín González

PII: S0268-005X(23)00960-8

DOI: https://doi.org/10.1016/j.foodhyd.2023.109414

Reference: FOOHYD 109414

To appear in: *Food Hydrocolloids*

Received Date: 1 June 2023

Revised Date: 5 October 2023

Accepted Date: 10 October 2023

Please cite this article as: Mercadal, P.A., Picchio, M.L., González, Agustí., Food-protecting films based on soy protein isolate and natural deep eutectic solvents: Antimicrobial and antioxidant properties, *Food Hydrocolloids* (2023), doi: https://doi.org/10.1016/j.foodhyd.2023.109414.

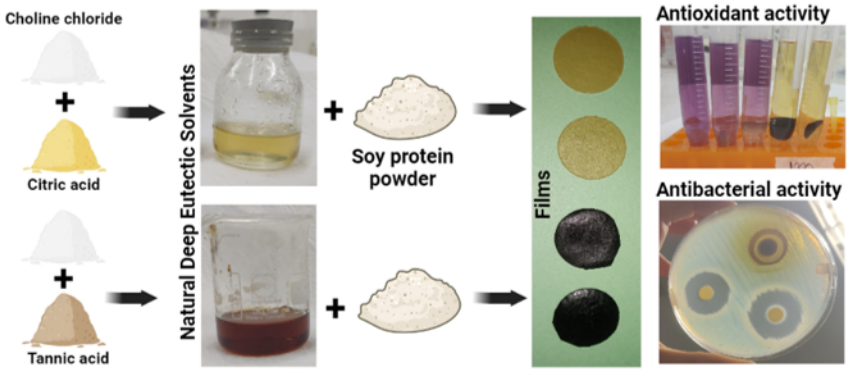

FOOD-PROTECTING FILMS BASED ON SOY PROTEIN ISOLATE AND NATURAL DEEP EUTECTIC SOLVENTS: ANTIMICROBIAL AND ANTIOXIDANT PROPERTIES

*Pablo A. Mercadal [a,b,c], Matias L. Picchio [d,e] and Agustín González [a,b]**

[a] Universidad Nacional de Córdoba, Facultad de Ciencias Químicas, Departamento de Química Orgánica, Córdoba (5000), Argentina.

[b] Instituto de Investigación y Desarrollo en Ingeniería de Procesos y Química Aplicada (IPQA-CONICET), Córdoba (5000), Argentina.

[c] Universidad Nacional de Córdoba, Facultad de Ciencias Agropecuarias, Departamento de Recursos Naturales, Córdoba 5000, Argentina

[d] Instituto de Desarrollo Tecnológico para la Industria Química (INTEC-CONICET), Santa Fe 3000, Argentina.

[e] POLYMAT, Applied Chemistry Department, Faculty of Chemistry, University of the Basque Country UPV/EHU, Donostia-San Sebastián 20018, Spain.

*Corresponding author: Agustín González

Email adress: agustingonzalez@unc.edu.ar

Postal address: Medina Allende y Haya de la torre, Ciudad Universitaria, Córdoba (5000), Argentina

Abstract

Natural deep eutectic solvents (NADES) have just recently emerged as promising plasticizers in food coating applications owing to their excellent anti-frosting properties, low cost, and biosafety. Herein, we report for the first time the use of NADES as bioactive additives of soy protein isolate (SPI) to fabricate functional packaging materials. A neoteric eutectic solvent based on choline chloride/ tannic acid (ChCl/TA) and the classical ChCl/citric acid mixture (ChCl/Cit) were explored to be integrated into the protein matrix at really high ratios (150 and 200 wt%). The resulting films were characterized by assessing morphological, physicochemical, and mechanical properties, as well as antioxidant and antimicrobial activities. The films exhibited a hydrophilic surface but limited water swelling (less than 10%), suggesting the formation of a crosslinked network between NADES and SPI. The ChCl/Cit films demonstrated potent antimicrobial activity in bacterial growth inhibition assay on chicken breast as well as in agar diffusion assays with inhibition zone diameters over 20 mm for gram+ and gram- bacteria, while ChCl/TA films showed the highest tensile strength (ranging from 744-2740 kPa), superior antioxidant activity (DPPH scavenging activity of ≈ 82%), and high light barrier properties, advantageous for storing light-sensitive food products. The incorporation of high concentrations of NADES in film production provides a novel and practical approach to improving the properties of protein materials for food packaging applications.

Keywords: Natural deep eutectic solvents; Isolated soy protein; Food packaging; Antibacterial activity; Antioxidant properties

1. Introduction

In recent years, deep eutectic solvents (DES) have gained prominence in green chemistry as promising alternatives to ionic liquids, as they offer several advantages, including biodegradability, low toxicity, and cost-effectiveness (Płotka-Wasylka, de la Guardia, Andruch, & Vilková, 2020). DES are composed of a hydrogen bond donor (HBD) and a hydrogen bond acceptor (HBA), forming a liquid mixture with an abnormal depression in its melting temperature (Wang, Zhang, Ma, & Yan, 2021). Within the family of DES, natural deep eutectic solvents (NADES) have garnered significant attention in food packaging applications due to their unique properties, such as anti-frosting, non-volatility, non-toxicity, and high biodegradability (Paiva et al., 2014). NADES are composed of natural components, commonly mixtures of choline chloride (ChCl) with organic acids (C. Florindo, Oliveira, Rebelo, Fernandes, & Marrucho, 2014), polyalcohols (L. P. Silva, Martins, Conceição, Pinho, & Coutinho, 2020), and sugars (Catarina Florindo, Oliveira, Branco, & Marrucho, 2017). Notably, a novel family of NADES has been recently reported based on ChCl and polyphenols, including tannic acid (TA), gentisic acid, and gallic acid, among others (Picchio et al., 2022). However, the full potential and functionalities of these innovative NADES remain largely unexplored, especially for film applications. For instance, the incorporation of ChCl/TA NADES into biopolymer materials could yield substantial enhancements in their mechanical properties, given by the multiple H-bond interactions of TA (P. Mercadal et al., 2023). In addition, TA could provide

antimicrobial and antioxidant activity, which is highly valuable for food-preserving coatings (Carnicero et al., 2022; Lee et al., 2023; Picchio et al., 2018).

The food packaging industry demands the incorporation of compounds or additives that prolongs the shelf-life of products while offering resistance, barrier properties, and non-toxicity to biodegradable materials (Casalini & Giacinti Baschetti, 2023; Sousa et al., 2022). The primary focus of food packaging research has been on advancing packaging methods that can enhance food preservation by interacting with the food product. These methods are referred to as "active packaging systems." Among the various types of active packaging, antimicrobial packaging stands out as a highly innovative and promising development in the past decade derived from the fact that the growth of bacteria on the surface of food is one of the factors that have the greatest influence on the loss of quality of the products and their end of useful life. For this reason, incorporating NADES with bioactive properties into food packaging materials could be a promising alternative to prevent product spoilage and effectively extend the shelf life of food (Vieira, de Carvalho, & Conte-Junior, 2022). Curiously, only a few research works have reported the development of packaging films utilizing NADES as active additives or plasticizing agents (Almeida, Magalhães, Souza, & Gonçalves, 2018; Galvis-Sánchez, Castro, Biernacki, Gonçalves, & Souza, 2018; Yu, Xu, Goksen, Yi, & Shao, 2023). The main research efforts have been put into studying the effect of NADES on chitosan films (Jakubowska, Gierszewska, Nowaczyk, & Olewnik-Kruszkowska, 2020; Wei Zhang, Shen, Gao, Jiang, & Xia, 2022) and a few other polysaccharides, such as locust bean gum (Grala et al., 2022), durian seed gum (Fang et al., 2022), and sodium

alginate (Tian, Sun, Xu, Fan, & Zhu, 2022). For instance, Yu *et al*. successfully produced chitosan films with enhanced mechanical properties incorporating ChCl-based DES and organic acids, resulting in films with antibacterial and antioxidant properties (Yu et al., 2023). In another study, Alves *et al.* employed NADES/green tea extracts to enhance the water barrier properties of chitosan films (Alves et al., 2022). Similarly, Jakubowska *et al*. prepared films by combining chitosan with NADES based on ChCl and citric acid (Cit), along with the addition of quercetin as an antioxidant additive (Jakubowska et al., 2020). However, the use of NADES as an additive in other types of biopolymer formulations, like proteins, for food packaging films has not been studied until now. SPI is a promising biopolymer for edible film production due to its biocompatibility, non-toxicity, and biodegradability. SPI produces flexible, more transparent, and softer films than those derived from other natural sources (Guilbert, Gontard, & Cuq, 1995). However, SPI based-films have limitations in terms of poor mechanical properties, susceptibility to moisture, low barrier properties, and no antimicrobial activity (Tao, Sedman, & Ismail, 2022). To address these shortcomings, several individual synthetical strategies were studied and various additives were assayed, such as the use of crosslinking agents (Azeredo & Waldron, 2016), the incorporation of nanoreinforcers (Hoyos-Merlano, Borroni, Rodriguez-Batiller, Candal, & Herrera, 2022) or different plasticizers (Ballesteros-Mártinez, Pérez-Cervera, & Andrade-Pizarro, 2020) for the improvement of mechanical and physicochemical properties, and the utilization of antimicrobial (Chawla, Sivakumar, & Kaur, 2021) or antioxidant (Manzoor, Yousuf, Pandith, & Ahmad, 2023) additives for obtaining active properties. In general, these works have successfully achieved individual improvements. However, incorporating

a single component has never accomplished the simultaneous enhancement of all these properties. NADES have demonstrated the capability to function as plasticizers (Alves et al., 2022; Jakubowska et al., 2020) upon their incorporation into bio-based films. Furthermore, it is expected that NADES that comprise constituents possessing crosslinking ability (Picchio et al., 2018), antimicrobial activity (L. Wen et al., 2021) and antioxidant potential (W. Liu et al., 2023), could confer these attributes to the films, simultaneously with their plasticizing effect. Motivated by this, this work aims to explore the utilization of NADES based on components with potential functional properties such as Cit (Wanli Zhang, Roy, Assadpour, Cong, & Jafari, 2023) and TA (Wanli Zhang, Roy, Ezati, Yang, & Rhim, 2023) to develop active films of SPI with improved physicochemical, thermal and mechanical performance.

Herein, we proposed for the first time the utilization of NADES based on ChCl/TA and ChCl/Cit as bioactive additives of SPI films for food packaging. The influence of incorporating these NADES at high ratios in the physicochemical properties of the films was investigated. In addition, the antibacterial and antioxidant activities of the films were evaluated. By exploring the potential of NADES in conjunction with SPI films, our research will contribute to the knowledge of the innovative and sustainable food packaging research field.

2. Materials and Methods

2.1 Chemicals

Tannic acid (Bio Pack, ≥99%); Choline chloride (Sigma Aldrich, ≥99%); anhydrous citric acid (Bio Pack, ≥99.5%); soy protein isolated (SPI) SUPRO E with 90% protein on a fat-free, dry-weight basis (DuPont, USA); NaOH pellets (Bio Pack, ≥97%); 2,2-Diphenyl-1-picrylhydrazyl, Trolox (Sigma Aldrich); Ethanol, $CaCl_2$ (≥99.5 % Cicarelli); Deionized water was used throughout the work.

2.2 Preparation of NADES

To obtain the NADES, the solid components (HBD/HDA) were mixed and heated at 95°C under constant stirring until form a homogeneous liquid. According to previous studies, NADES were prepared using a 2:1 molar ratio of ChCl/Cit (Smirnov et al., 2021) or a 20:1 molar ratio of ChCl/TA (Picchio et al., 2022).

2.3 Synthesis of Films

The protein films were prepared by the casting method. To this, 1.2 g of the film-forming SPI was dissolved in 45 mL of water at room temperature. Then, ChCl/TA or ChCl/Cit NADES were added (1.8 g or 2.4 g) to achieve 150 and 200 wt% of each type of NADES based on the SPI. The resulting dispersions had pH values of around 4 and were mixed at room temperature for 4 h. The pH value of the mixture containing ChCl/TA was then adjusted to 8 by adding NaOH 5 M. The solutions were poured into plastic Petri dishes with an area of 63.6 cm^2 and left to dry for 24 h at 60°C. Then, the films were cooled at room temperature and peeled off the plate. A

158 sample control was prepared by adding 0.6 g of glycerol to 1.2 g of SPI dissolved in
159 45 mL of water to obtain standard SPI film with 50 wt% of glycerol based on SPI.

160

161

162 *2.4 Thickness determination*

163 The film thickness was determined as the average of 10 measurements for each
164 sample using a hand-held micrometer (model ESP1-0001PLA, Schwyz, Swiss). The
165 average thickness was used for assessing mechanical properties, water vapor
166 permeability, and opacity properties.

167 *2.5 Determination of moisture content and total soluble matter*

168 The moisture content (MC) and total soluble matter (TSM) of the films were
169 determined using the methodology described in the literature (Rhim, Gennadios,
170 Weller, Carole Cezeirat, & Hanna, 1998). To measure the MC, portions of each film
171 were weighed (W_0) on glass plates, dried in an oven at 110 °C for 24 hours, and
172 weighed again (W_i). The MC values were calculated in triplicate using Eq. 1:

173 $$MC = [(W_0 - W_i) / W_0] \times 100\% \quad (1)$$

174 For TSM measurements, each film with mass W_0 was immersed in beakers
175 containing 30 mL of distilled water for 24 hours, then dried at 110 °C for 24 hours
176 and weighed (W_f). The TSM values were determined in triplicate using Eq. 2:

177 $$TSM = [(W_i - W_f) / W_i] \times 100\% \quad (2)$$

Note that the W_0 values for MC and TSM experiments are almost the same (±0.5 mg).

2.6 Measurement of the filmogenic solution viscosity

The viscosity of SPI solutions before and after adding NADES was determined at 25 °C using a Brookfield viscometer (Advance series, ADVL 101021, FUNGILAB INC, New York, USA). The measurements were performed in a range from 5 to 100 r.p.m, using a plate spindle of 15 mm in diameter and after one minute of starting the assay. Each measurement was recorded in sextuplicate.

2.7 Contact angle measurements

The contact angle measurements were conducted at 25 °C using a homemade contact angle goniometer by the Sessile Drop method (Romero, Wolfel, & Igarzabal, 2016). A drop of 4.00 ± 0.04 mm^3 of Milli-Q water was dispensed onto the film surface using a syringe, with a 4.00 ± 0.01 mm distance between the needle tip and the film surface. During the experiment, a video was recorded with a Logitech c922 digital camera and processed using the native video player software of Windows 10. For each sample, the frame captured 1 second after the drop came into contact with the film surface was selected and analyzed using IMAGEJ 1.4 software. All measurements were performed in seven different locations on each sample.

2.8 Swelling test

The water uptake ($S\%$) of the different samples was calculated using the following equation (González, Gastelú, Barrera, Ribotta, & Álvarez Igarzabal, 2019):

$$S\% = [(W_s - W_0)/W_0] \times 100\% \quad (3)$$

where W_0 is the initial weight of the samples and W_s is the weight after immersion in 30 mL of deionized water for specific time intervals at room temperature. The W_s values were recorded after removing the samples from the swelling medium and drying the surface with tissue paper to absorb any excess water. All measurements were performed in triplicate.

2.9 Water Vapor Permeability test

Water vapor permeability (WVP) was determined in duplicate for each film following the desiccant procedure described by the ASTM standard method E96M-10 (ASTM, 2010). The films were placed in a humidity chamber at 30 °C and 70% relative humidity (%RH) for one day to reach equilibrium. Subsequently, the films were fixed onto aluminum capsules (50 mm diameter, 17 mm depth) containing anhydrous $CaCl_2$ (dried at 180 °C for 24 hours) and sealed with silicone grease. The desiccant was separated from the atmosphere by the film. These capsules were weighed and placed in a humidity-controlled chamber under the same conditions as those in which the films were previously conditioned. The weight variation of the entire system was recorded every hour up to 12 measurements. These values were plotted as weight variation versus time, obtaining a linear function. Water vapor transmission (WVT) was calculated using Equation 4:

$$WVT = F/A \quad (4)$$

where F and A are the slope of the linear function and the surface area exposed, respectively. Then, WVP was calculated according to Equation 5:

$$WVP = (WVT \times e)/S \times (RH_1 - RH_2) \times 3600 \quad (5)$$

where e is the film thickness, S is the saturation pressure at 30 °C and $(RH_1 - RH_2)$ is the difference between the relative humidity inside the chamber (RH_1 = 0.7, since the %RH of the chamber is 70%) and the relative humidity inside the capsule (RH_2 = 0, since the %RH inside the capsule is 0% due to the presence of anhydrous $CaCl_2$).

2.10 Opacity

Each film was cut in a 2.5 x 1.0 cm rectangle. Opacity was determined by calculating the area under the absorbance curve in the visible spectrum (400 to 800 nm) for each sample. The area values were normalized by dividing them by the thickness of each film.

2.11 Thermal properties

Differential scanning calorimetry (DSC) analyses of the films, NADES and SPI were performed on a 2920 Modulated DSC (TA Instruments, USA). 5 mg of each sample was sealed in a hermetic aluminum pan and heated from -40 to 250 °C at a rate of 10 °C/min. A nitrogen flow (50 mL/min) was maintained during the entire test. The

thermogravimetric analysis (TGA) was performed in a Hi-Res Modulated 2950 Thermogravimetric Analyzer (TA Instruments, USA) at 10 °C/min from 25 °C to 600 °C.

2.12 FTIR analysis

The films were characterized using attenuated total reflectance-Fourier transform infrared spectroscopy (ATR-FTIR) with a Nicolet 5-SXC spectrometer coupled to a Nicolet iN10 microscope (Thermo Scientific, USA) and a ZnSe crystal with an incidence angle of 45°. To ensure the homogeneity of each sample, different areas of the films were analyzed. The NADES and SPI powder spectra were recorded in reflection mode by depositing the sample on a gold mirror and collecting an average of 32 scans with 4 cm^{-1} resolution, with air as the background.

2.13 Morphological Characterization

The surface morphology of the different films was studied by scanning electron microscopy (SEM). Films were attached to a double-sided carbon adhesive tape mounted on SEM stubs, coated with chrome under a vacuum, and examined with an SEM microscope (Carl Zeiss - Sigma, Germany). SEM images were acquired at a magnification of 200x, an aperture size of 30 μm, electron high tension (EHT) of 3 kV, and a working distance of 4 mm.

2.14 Mechanical properties

The mechanical properties of the films were determined by the tensile test according to American Society for Testing and Materials D882-02 (ASTM, 2002) in quintuplicate on an Instron Universal Testing Instrument (model EMIC 23-5S, Instron, USA) equipped with a 50 N load cell. Briefly, samples were cut into rectangles of 70x20 mm and subjected to controlled deformation while the stress-strain curves were recorded. The initial separation was set at 50 mm, and a crosshead speed of 0.1 $mm.s^{-1}$ was used. Using the sample dimensions and the stress-strain curve generated from the recorded load and extension, the Tensile Toughness values were calculated by determining the area under the stress-strain curves as follows (Kovačič, Žagar, & Slugovc, 2019):

$$\text{Tensile Toughness} = \int_0^{\varepsilon f} \sigma_e d\varepsilon_e \quad (6)$$

where σ_e is the stress ($N.m^{-2}$), ε_e the strain (unitless), and εf is the fracture strain of the sample, respectively.

2.15 Antibacterial activity by agar diffusion assay

The antibacterial activity of films was tested with the agar diffusion assay described by Carnicero *et al.* (Carnicero et al., 2022). The bacterial strains used were *Escherichia coli* ATCC 25922, *Staphylococcus aureus* ATCC 25923, *Pseudomonas aeruginosa* PA01, and *Enterococcus faecalis* ATCC 25212. The films were cut into 8 mm diameter discs and then arranged in Petri dishes containing Brain-heart agar previously inoculated with the microorganism by raking to assess inhibition of

bacterial growth. Each inoculum was previously carried out by suspension in a phosphate buffer dilution of the respective bacteria, taken from a pure fresh culture of up to 48 h of incubation after ringing. Afterward, sterilized forceps were used to place the film samples on the inoculated plate in the laminar airflow chamber. Thereafter, the plates were incubated at 37 °C for 24 h. After incubation, the diameter (mm) of the inhibition zone around each disc was calculated. The measurements were done in triplicate for each film.

2.16 Antibacterial activity on chicken breast

Film samples (5 × 5 cm) were used for cover the surface of pieces of fresh chicken breast, using as control samples a film without NADES but with glycerol at 50 wt% and a piece of chicken breast without film. The count of microorganisms was carried out for fresh chicken breast and after 4 days of storage at 4 °C, employing the methodologies reported by Compendium of Methods for the Microbiological Examination of Foods (Salfinger & Tortorello, 2015). The tests were carried out by removing the film and swabbing the surface of the food, then this swab was washed in a final volume of 20 mL of sterile phosphate buffer. A sterile petri dish was inoculated with 1 mL of the buffer and then a layer of violet-red bile Glucose Agar (VRBG) for *Enterobacteriaceae* (ENT) or Violet Red Bile Agar (VRBL) for *total coliforms* was added. The inoculum was homogenized with the melted agar, allowing the medium to solidify on a flat surface and a second layer of medium was added. The plates were incubated at 36 ºC for 48 h and the colonies were counted. For the count of *E. coli* and *aerobic mesophilic bacteria* (AMB), the same procedure as

mentioned was used but employing Chromagar ECC (*E. coli)* or Plate count agar (AMB). The plates were placed inverted in the oven and incubated at 44 ºC for 24 h (*E. coli*) or 36 ºC for 48 h (AMB) and the typical colonies formed were counted. For *S. aureus* the surface seeding technique was used, inoculating 0.4 mL of the washing buffer on a plate with Baird Parker. The inoculum was homogenized on the surface with a Drigalsky spatula previously sterilized by flame. The plates were placed inverted and incubated at 36 ºC for 48 h and then the colony count was carried out. All the assays were performed in duplicate and the results were expressed as log_{10} CFU/cm^2.

2.17 Antioxidant Activity

Film samples were cut into small pieces weighing 100 mg. For 2,2-diphenyl-1-picrylhydrazyl (DPPH) radical scavenging activity (DPPH-RSA), the film's pieces were submerged in 10 mL of 1x10^{-4} M DPPH solution in 99.5% ethanol. The mixtures were gently mixed and allowed to stand at room temperature in the dark for 1 hour. The absorbance of the resulting solution was measured at 517 nm using a Shimadzu 1800 spectrophotometer. A standard curve was prepared using Trolox in the range of 1.6–30 μM. The activity was calculated from the equation generated from the standard curve and expressed as μmol Trolox equivalents (TE)/g sample according to Gulzar *et al.* (Gulzar, Tagrida, Nilsuwan, Prodpran, & Benjakul, 2022). In order to perform a comparison with other research in literature, antioxidant capacity is also informed as DPPH scavenging activity (%) and calculated as Eq. 6.

$$\text{DPPH scavenging activity } (\%) = \left(\frac{Ac-As}{AC}\right) \times 100\% \quad (7)$$

where As indicates the absorbance of the sample, Ac indicates the absorbance of the control (containing only DPPH solution) with ethanol at 517 nm wavelength.

2.18 Statistical analysis

Data for each test were statistically analyzed. The analysis of variance (ANOVA) was used to evaluate the significance of the difference between means. Turkey test was used for comparing mean values; differences between means were considered significant when $P \leq 0.05$.

3. Results and Discussion

3.1 Preparation of NADES and films

As displayed in Fig. 1A, the synthesized ChCl/Cit and ChCl/TA NADES were homogeneous liquids at room temperature with suppressed melting point (Fig. S1) in agreement with the literature (Picchio et al., 2022; Smirnov et al., 2021), confirming the successful preparation of the NADES. After that, they were incorporated into SPI solutions in different proportions from 70 to 250 wt%. Curiously, NADES amounts lower than 150 wt% resulted in very brittle materials, while concentrations above 200 wt% did not form self-standing films. Compared with typical protein plasticizers such as glycerol, where concentrations of 30 wt% are enough to obtain flexible films, ChCl/Cit and ChCl/TA NADES seem less effective in reducing the interactions between SPI chains. Far from being a negative point for

these systems, this lower plasticizing effect eventually implies loading the films with much more bioactive components (TA or Cit contained in the plasticizing NADES), otherwise impossible with traditional plasticizing agents due to solubility limitations, boosting the films' functionality.

SPI solutions containing ChCl/TA were adjusted to pH 8 (pKa of TA ~ 8.5) to promote intra- and inter-molecular hydrogen bonding, which is facilitated by the unfolding of SPI proteins under alkaline conditions, as reported by Guerrero *et al.* (Guerrero & de la Caba, 2010). Unfortunately, SPI solutions containing ChCl/Cit precipitated at pH 8, probably due to protein destabilization by ionic interactions (pKa of Cit 3.15, 4.77, and 6.40); thus, in this case, films were prepared without modification of the pH. Positively, it is well-known that antibacterial properties are enhanced at acidic pH (Salihu et al., 2021).

Viscosity measurements of the SPI dispersions before and after adding NADES were measured, showing a decrease in the viscosity values as the shear rate increases (Fig. S2), in agreement with the reported by Liu *et al.* (P. Liu, Xu, Zhao, & Yang, 2017). The slight decrease in the viscosity values of the SPI solutions after adding NADES is probably associated with a dilution effect of the protein dispersion.

Films were prepared as was explained in section 2.3. Fig. 1B shows that films with 150 or 200 wt% of ChCl/Cit (F-150% ChCl/Cit or F-200% ChCl/Cit) were yellowish, while films with 150 or 200 wt% of ChCl/TA (F-150% ChCl/TA or F-200% ChCl/TA) were brownish. All prepared films show homogeneous colors indicating a good dispersibility of NADES without phase separation despite their high concentration. The average thickness values of films were 415 ± 33, 589 ± 12, 531 ± 36, and 570

375 ± 28 μm for F-150% ChCl/TA, F-200% ChCl/TA, F-150% ChCl/Cit and F-200%
376 ChCl/Cit, respectively. It is worth mentioning that films were not correctly formed if
377 ChCl and TA or Cit powders were directly added to the SPI solution to obtain ratios
378 of 150 and 200 wt% instead of adding the prepared NADES (Fig. S3).

379

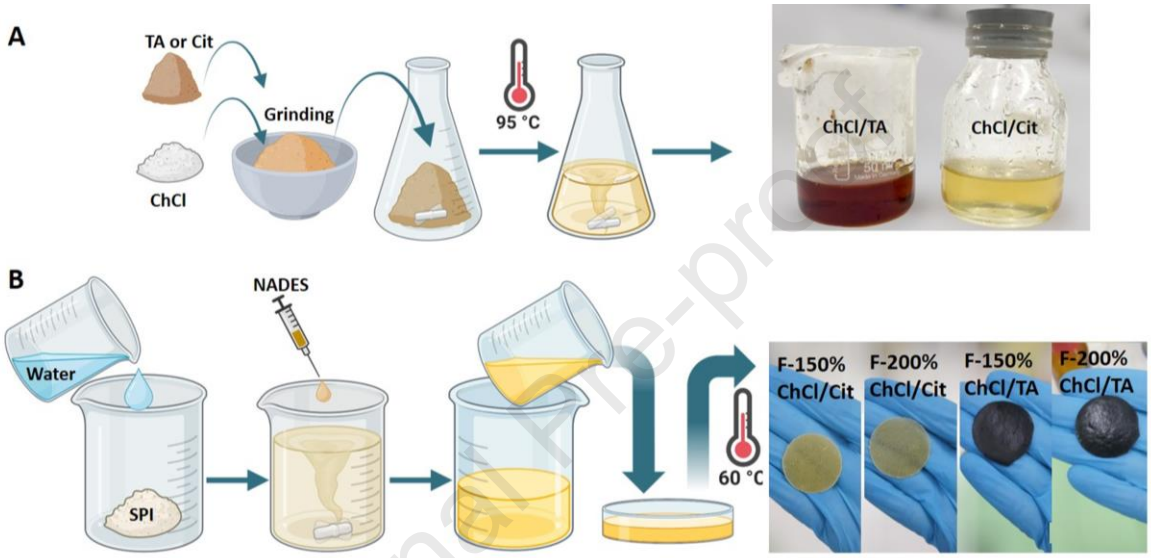

380

381 **Fig. 1.** Schematic illustrations of ChCl/TA or ChCl/Cit formation (**A**) and the process for obtaining the
382 films with different ratios of ChCl/TA or ChCl/Cit (**B**).

383

384 *3.2 Fourier transform infrared (FTIR) spectra*

385 The chemical characterization of SPI, NADES, and films was performed using ATR-
386 FTIR spectroscopy. Since the studied systems present a great complexity and
387 variety of functional groups, very wide absorption bands are observed in all the
388 spectra. The black line in Fig. 2 shows the typical FTIR spectrum of SPI powder,
389 where the characteristic band centered at 3301 cm^{-1} corresponding to free and
390 bound O-H and N-H groups could be observed. Notably, this band is more intense
391 and remarkably shifted to higher wavenumbers in ChCl/TA films spectra (Fig. 2A),

whereas it is subtly shifted to lower wavenumbers in ChCl/Cit-containing films (Fig. 2B). The same trend is observed for the band located at 1630 cm^{-1} assigned to C=O stretching peak of amide I in SPI. These shifts are attributed to the interaction between TA (Picchio et al., 2018) or Cit (Yu et al., 2023) with SPI. The remarkable shift of the band in the case of ChCl/TA films is in line with previous literature on the crosslinking of SPI by phenolic acid (Kang, Wang, Zhang, Li, & Zhang, 2016) and schematized by Picchio *et al.* (Picchio et al., 2018) and Straus *et al.* (Strauss & Gibson, 2004), as shown in Fig. S4A, which illustrates the interaction between TA and SPI protein. In addition, the crosslinking mechanism for the ChCl/Cit film involves H-bonding (Fig. S4B), following the scheme proposed by Wei *et al.* for chitosan and ChCl/urea DES (Wei et al., 2023). The characteristic C-H stretching of CH_2 and CH_3 groups of saturated structures are observed in the range 2980-2850 cm^{-1} in SPI and the films spectra but not in ChCl/TA (Fig. 2A, red line) and ChCl/Cit (Fig. 2B, orange line) NADES spectra. The peak at 1730 cm^{-1} observed in both NADES spectra is attributed to the stretching of the C=O bond, and it is present in all fabricated films but exhibits greater intensity for those obtained with ChCl/Cit than ChCl/TA. Furthermore, regardless of the type of NADES employed, this peak shows a lower relative intensity in the films with 150 wt% NADES compared to the 200 wt% films due to the higher concentration of eutectic solvent (Jakubowska et al., 2020). The peak at 1234 cm^{-1} in the SPI spectrum is attributed to the C-N stretching and N-H bending (amide III) vibrations, while the peak at 1050 cm^{-1} corresponds to C-O stretching, which are also observed in FTIR spectra of films with both NADES (Erdem & Kaya, 2021; Schmidt, Giacomelli, & Soldi, 2005). Finally, a peak at ~ 950

415 cm^{-1} in both NADES spectra, attributed to C-C-O vibrations, was present in the
416 prepared films.

417

418 .

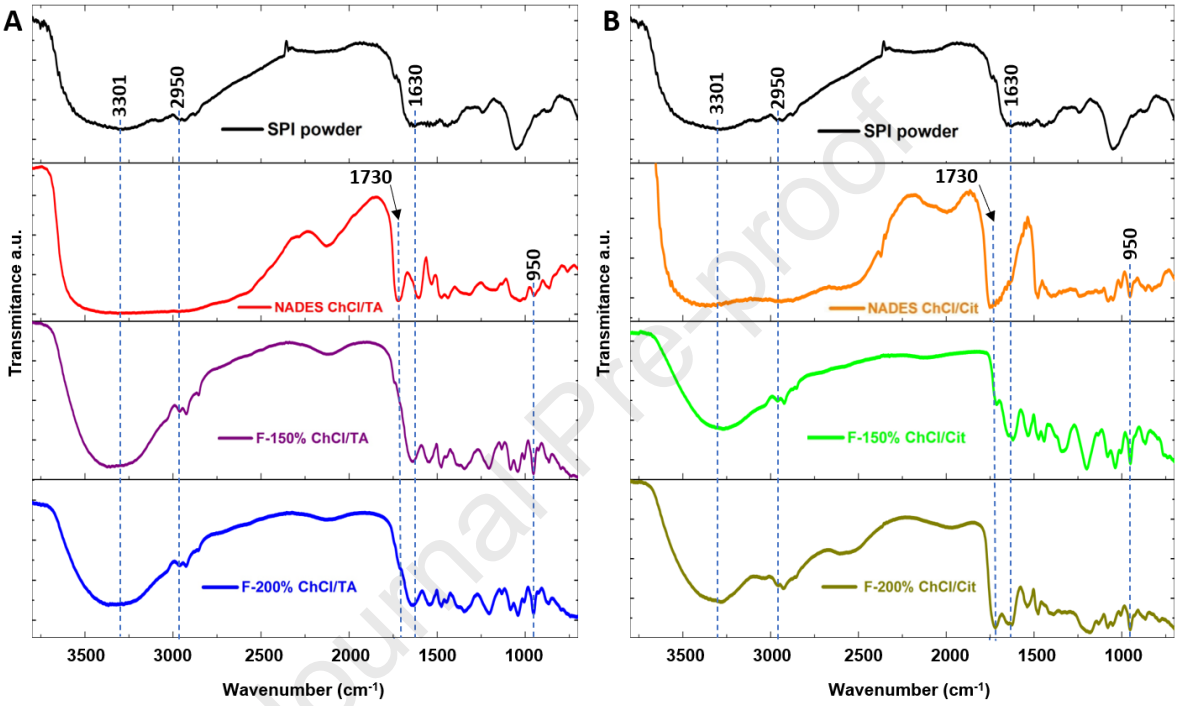

419

420 **Fig. 2.** FTIR spectra of SPI powder, pure NADES, and the as-prepared films based on ChCl/TA (**A**),
421 and ChCl/Cit (**B**).

422

423 *3.3 Morphology*

424 The morphological characterization of the films was performed by acquiring SEM
425 images of circular samples. The SEM images of F-150% and F-200% ChCl/Cit
426 display a rough surface with grain-like features (Fig. 3A and B). The SEM image of
427 F-150% ChCl/TA shows the surface of the film without the presence of pores, cracks,
428 or fissures but with unsolved material (Fig. 3C). These features are also observed in
429 the SEM image of F-200% ChCl/TA, where the amount of unsolved material

becomes more noticeable due to the high amount of ChCl/TA (Fig. 3D). The variation in the surface characteristics between the grain-like texture observed in films produced with ChCl/Cit and the surface of ChCl/TA samples can be attributed to the difference in fabrication conditions. The films with ChCl/TA are formed at a pH ≈ 8, while those with ChCl/Cit are at a pH ≈ 4. This difference in pH levels influences the aggregation of the SPI protein, resulting in distinct surface textures (Gennadios, Brandenburg, Weller, & Testin, 1993; Guerrero & de la Caba, 2010).

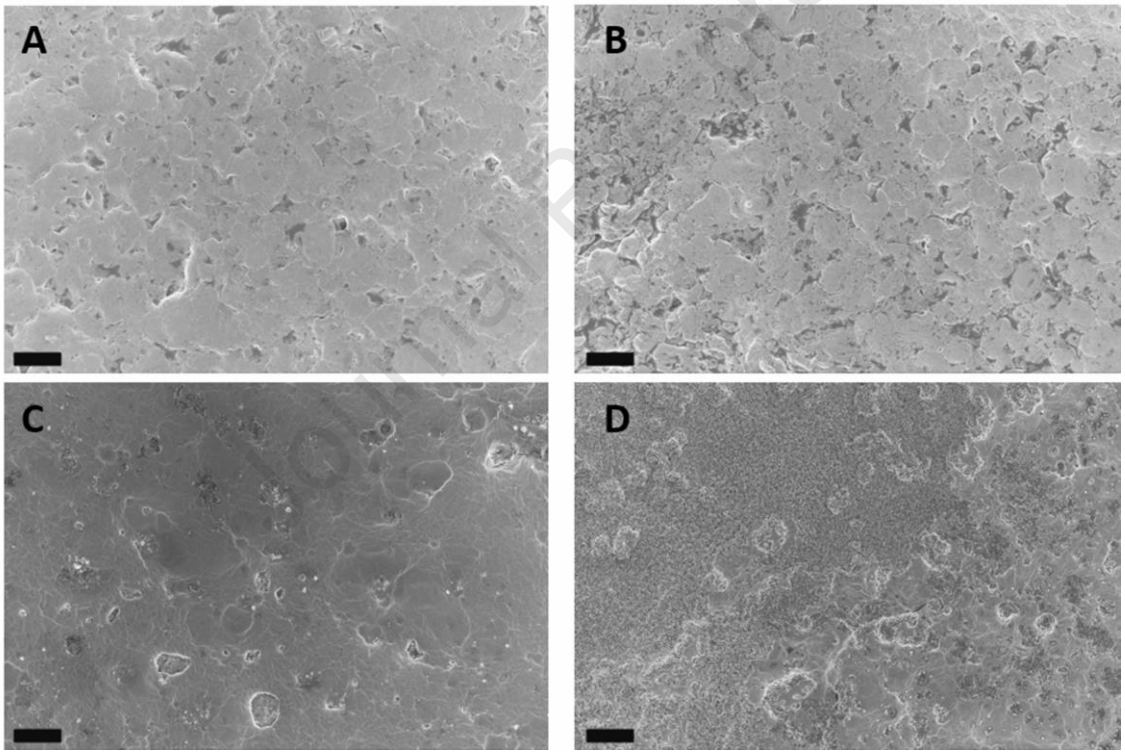

Fig. 3. SEM images of F-150% ChCl/Cit (**A**), F-200% ChCl/Cit (**B**), F-150% ChCl/TA (**C**) and F-200% ChCl/TA (**D**). The scale bar is 50 μm.

3.4 Thermal properties

The thermal properties of SPI powder, NADES, and films were analyzed using TGA and DSC assays. The TGA of the SPI powder (Fig. 4A and B, black lines) showed a

445 rapid weight loss up to 120 °C due to water evaporation, followed by a single event
446 at 306 °C that agrees with their maximum degradation temperature ($T_{dmax\%}$) value
447 obtained from the derivative weight curve (Table 1 and Fig. 4C and D). The thermal
448 decompositions of ChCl/TA (Fig. 4A, red line) and ChCl/Cit (Fig. 4A, orange line)
449 showed simple profiles according to previous works (Picchio et al., 2022; Pontillo,
450 Koutsoukos, Welton, & Detsi, 2021). Additionally, the fact that NADES degradations
451 occur at relatively high temperatures indicates their good thermal stability. The
452 degradation temperature at 5% ($T_{d5\%}$) of ChCl/TA and ChCl/Cit appeared at 125 and
453 171 °C, while 50% of weight loss ($T_{d50\%}$) occurred at 279 and 242 °C, respectively
454 (Table 1 and Fig. 4C and D). As displayed in Fig. 4A, purple and blue lines, shows
455 films with ChCl/TA have a similar decomposition profile to pure ChCl/TA NADES but
456 with different weight loss proportions. The $T_{d5\%}$ values of F-150% ChCl/TA (64 °C)
457 and F-200% ChCl/TA (116 °C) were lower than that of ChCl/TA NADES (125 °C)
458 due to water evaporation from the films. Conversely, $T_{d50\%}$ values of ChCl/TA films
459 shifted to higher temperatures than the pure NADES (Table 1 and Fig. 4C and D),
460 attributed to the decomposition of crosslinked structures given by dynamic
461 interactions between TA and the protein (P. A. Mercadal et al., 2023). Films
462 fabricated with ChCl/Cit show a similar decomposition profile to those prepared with
463 ChCl/TA. In this case, the dynamic crosslinked structures result from the interactions
464 between SPI's OH and NH_2 groups with the carboxylic groups of citric acid (Smirnov
465 et al., 2021).

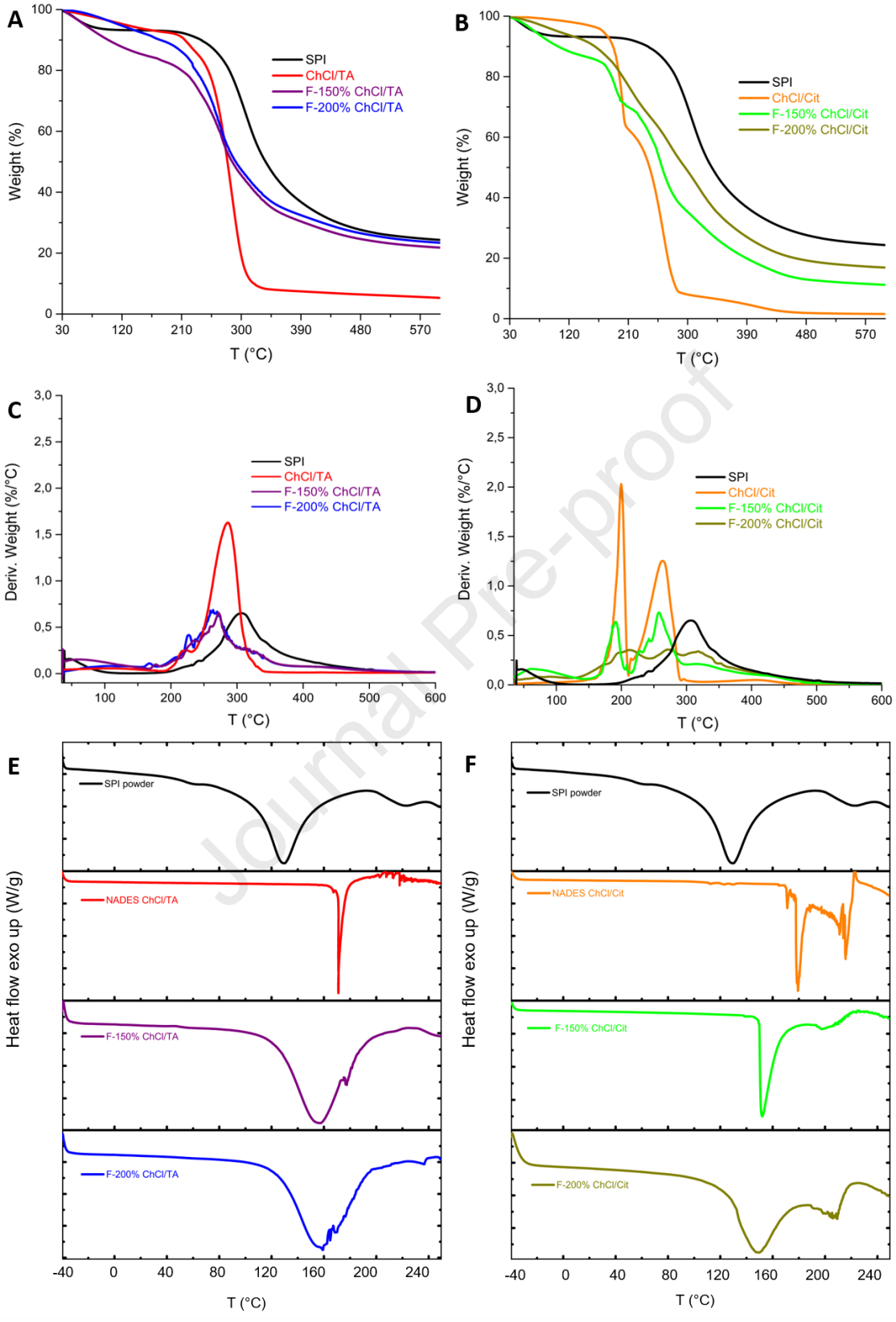

Fig. 4. TGA curves (**A** and **B**), calculated derivative weight %/°C (**C** and **D**) and DSC scans upon the first heating cycle (**E** and **F**).

469 **Table 1.** Thermal Properties of the SPI powder, NADES, and films

Samples	$T_{d5\%}$ (°C)	$T_{d50\%}$ (°C)	$T_{dmax\%}$ (°C)	T_{end} (°C)
SPI	67	336	306	125
ChCl/TA	125	279	285	171
F-150% ChCl/TA	64	286	270	157
F-200% ChCl/TA	116	291	267	155
ChCl/Cit	171	242	263	179
F-150% ChCl/Cit	68	261	258	152
F-200% ChCl/Cit	103	296	272	150

470

471 The DSC analysis of the SPI powder's heating ramp indicates three characteristic
472 peaks (Fig. 4E and F, black lines). The primary endothermic peak, with a maximum
473 of 125 °C, is attributed to the denaturation of glycine protein fraction and loss of
474 residual water. The minor peaks at 62 and 224 °C correspond to the denaturation of
475 β-conglycinin and loss of the most stable immobilized water, respectively (Hu et al.,
476 2009; Tang, Choi, & Ma, 2007). The fifth column of Table 1 displays the temperature
477 values of the primary endothermic peaks (T_{end}) for SPI, NADES and the prepared
478 films. The DSC scan of ChCl/TA (Fig. 4E, red line) and ChCl/Cit (Fig. 4F, orange
479 line) shows good thermal stability of the compounds up to 150 °C. After 150°C, the
480 observed endothermic peaks of NADES are due to their decomposition, according
481 to TGA results and previous reports (Craveiro et al., 2016; Shafie, Yusof, & Gan,
482 2019). The glass transition temperature of NADES was not observed because it was

reported to be around -60 °C (Picchio et al., 2022), which is below the DSC measuring temperature range.

The DSC analysis of F-150% ChCl/TA (Fig. 4E, purple line) shows an endothermic broad and strong peak (157 °C) shifted to a lower temperature than the pure NADES (Zdanowicz, Spychaj, & Mąka, 2016). Meanwhile, the appearance of this peak is at a higher temperature than SPI due to the hydrogen bond interaction with TA to form a crosslinked network. Similarly, F-200% ChCl/TA (Fig. 4E, blue line) exhibits an endothermic peak as F-150% ChCl/TA but located at 155 °C. Films fabricated with ChCl/Cit follow almost the same thermal trend as above (Fig. 4F, green, and gold lines). However, in this case, the shift of the endothermic peak to lower temperatures than pure ChCl/Cit is more prominent probably due to a weak crosslinked network.

3.5 Mechanical properties

The stress vs. strain curves for the films are presented in Fig. 5A. It is noticeable that the films prepared with ChCl/TA demonstrated superior mechanical properties compared to those made with ChCl/Cit. This is attributed to the multiple dynamic interactions provided by TA, which results in a more robust physically crosslinked network (P. A. Mercadal et al., 2023). Specifically, F-150% ChCl/TA displays tensile strength and elongation at break values of 2750 kPa and 70%, respectively (Fig. 5B). As expected, the NADES exerts a plasticizer effect since F-200% ChCl/TA has lower tensile strength and elongation at break values (750 kPa and 45%, respectively), making it a less resistant material than F-150% ChCl/TA (Fig. 5B). A similar trend is observed for the films prepared with ChCl/Cit, as increasing the

amount of NADES results in a decrease in the final mechanical properties of the material. Furthermore, Young's modulus and toughness values were similar, regardless of the NADES type used (Fig. 5C). The decrease in the mechanical properties as the content of NADES increases could not be attributed only to the plasticizer effect of the eutectic solvent since the elongation at break should be higher for samples with 200 wt% of NADES. We surmise that this effect could also be attributed to a greater presence of aggregates, as was shown in SEM images (Fig. 3), which produce inhomogeneities in the protein matrix. This finding is in line with Pontillo *et al*., which reported a similar behavior for chitosan films plasticized with NADES based on ChCl and betaine/lactic acid at different concentrations (Pontillo et al., 2021).

It is worth mentioning that depending on the type of NADES employed, we observed different degrees of the detriment of the mechanical properties when the content of this component increased from 150 to 200%. An opposing effect is observed between the plasticizing behavior of NADES and the crosslinking effect generated by TA and Cit. In the case of films containing ChCl/TA at 150%, it could be expected that a significant number of interactions between TA and SPI chains occur, yielding a pronounced crosslinking effect. As the amount of NADES increases to 200%, the contribution of the plasticizing effect predominates over the TA crosslinking effect, decreasing the mechanical parameters, probably due to a saturation of the moieties of SPI protein. This behavior is much less pronounced for films containing NADES with Cit since the crosslinking effect of this molecule is substantially lower than that of TA, leading to minimal changes in the mechanical properties when the solvent

content is increased. Finally, we analyzed the eutectic films' behavior against a control sample of SPI and glycerol (50 wt%), finding that F-150% ChCl/TA shows superior tensile strength (Table S1). However, increasing NADES concentrations led to a detriment in the mechanical properties compared with the control, indicating that the plasticizing effect in F-200% ChCl/TA and Ch/Cit was more important than that provided by glycerol.

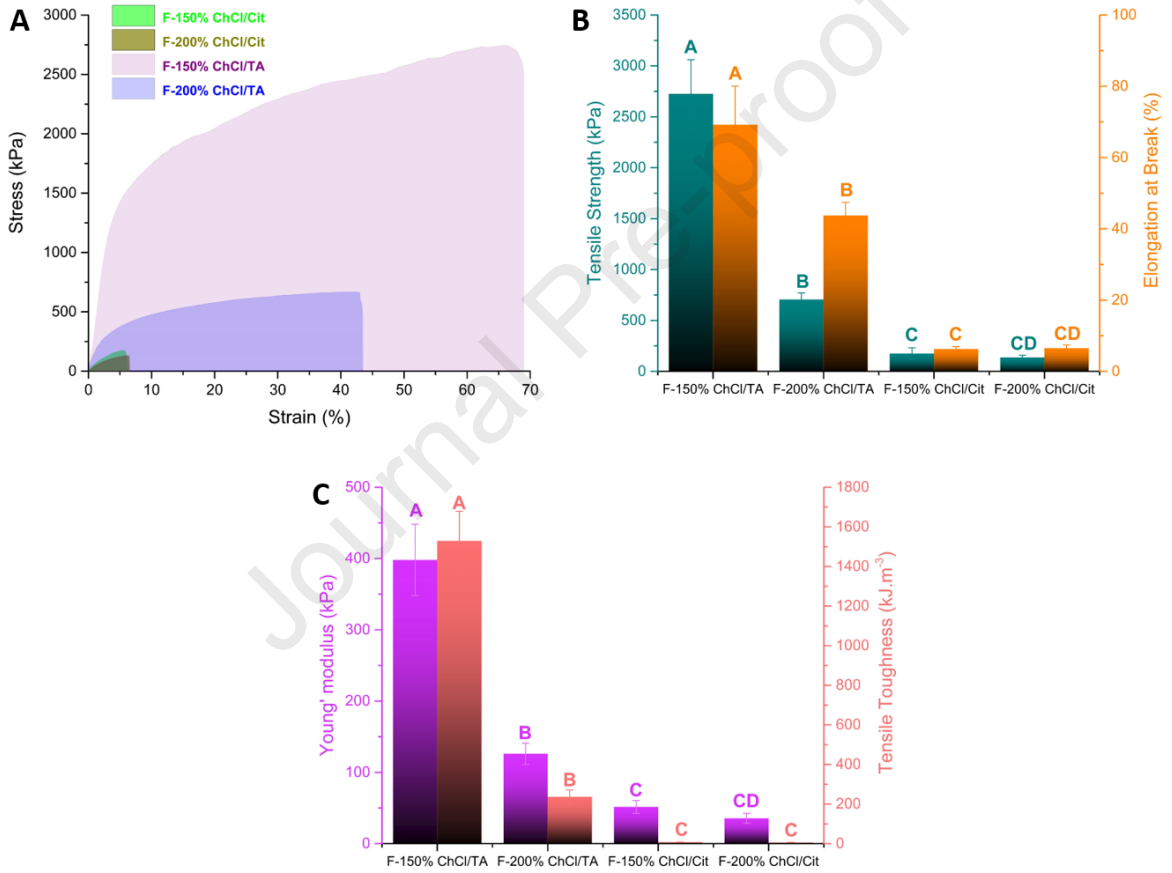

Fig. 5. (**A**) Stress vs. strain curves of the films. (**B**) Tensile strength (green column) and elongation at break (orange column) values of films. (**C**) Young's modulus (pink column) and toughness (ruby column) values of the films. Two values in the same column followed by the same letter are not different ($p \geq 0.05$) according to the Tukey test.

3.6 Physicochemical properties and opacity

The water contact angle values of the prepared films were approximately 45°, with no significant differences between samples (Fig. 6A), so it can be concluded that it is not affected by the NADES components or their concentration. This result indicates that the surfaces of the films are hydrophilic, as expected, given the polar nature of the NADES and SPI. The values of the contact angle of these SPI films are similar to those of films prepared with glycerol as a plasticizer (44°) (González, Barrera, Galimberti, Ribotta, & Alvarez, 2019). The hydrophilic surface of the films could limit their applications in contact with wet-surface materials such as food. Nevertheless, this seems not to be an overcome since the films showed relatively low swelling values. As shown in Fig. 6B, all films show low swelling values within 72 h of immersion in deionized water. This low swelling suggests that NADES promote multiple interactions, forming a more compact, and crosslinked network with polar groups interacting with each other and restricting the interactions with water. It is highlighted that the swelling curves have 2 stages. The first stage corresponds to a gradual increment of the water sorption over time until it reaches a maximum value at a specific point, depending on the NADES type and concentration. The second stage begins after the films reach the maximum swelling values, evidenced by a negative slope in the water uptake. This behavior is due to the presence of soluble matter that increases as the content of NADES increases, which favors the dissolution of the films or NADES diffusion to water, as shown in Fig. 6C. The swelling index values of SPI film (control film) was markedly higher than films containing NADES. Considering that the contact angle values were similar for these materials (Table S1), we can affirm that this lower swelling value is probably due to

a crosslinking effect in the NADES-containing films. TSM data showed larger values for ChCl/Cit than ChCl/TA films since TA produces a more compact and crosslinked network than Cit derived from the more significant number of interactions that can provide with the protein. Concerning the amount of NADES incorporated into the films, it could be observed that an increase in the NADES proportion produces an increase in the TSM derived from the greater diffusion of this solvent to the medium. On the other hand, the MC values did not show statistical differences between samples.

The water barrier properties of films are important in food packaging applications, particularly for preserving foods with large amounts of water and predicting the stability and quality changes during the processing and storage stages. As shown in Fig. 6D green columns, WVP values were extraordinarily low, in the range of 1-3 $\times 10^{-13}$ g/Pa.s.m^2, due to the high concentration of NADES. It is worth noting that these WVP values are orders of magnitude lower than those of similar films fabricated with NADES (Galvis-Sánchez et al., 2018; Pontillo et al., 2021; Zhao et al., 2022). In addition, WVP value of the control SPI films (50 wt% glycerol) is 100 times higher than the SPI films fabricated with NADES (Table S1). Regardless of the NADES type, the WVP decreases as the solvent content decreases. Besides, the values for the film containing ChCl/TA are smaller than that of ChCl/Cit, supporting again that the crosslinking effect of TA is greater compared to Cit. This result suggests smaller interstitial spaces between the biopolymer chains, which agrees with SEM images where more compact structures were observed for F-150% than F-200% films. It is highlighted that, despite the rough and heterogeneous surface of

the films, their low water vapor permeability values support the hypothesis of a continuous structure without any significant breaches or perforations.

On the other hand, opacity is a feature that may be advantageous for packaging foods that are sensitive to light, such as some fruits and fish (Oliveira Filho et al., 2019). In this sense, the SPI films with ChCl/TA have much higher opacity values than SPI films with ChCl/Cit, given by the characteristic dark/brown color of TA (Fig. 6D, brown color), and non-significant statistical differences were observed when varying the content of each NADES. Furthermore, the opacity values of these films were higher than native SPI films with 50 wt% glycerol (Table S1) due to the yellowish and brownish colors of ChCl/Cit and Ch/TA NADES, respectively.

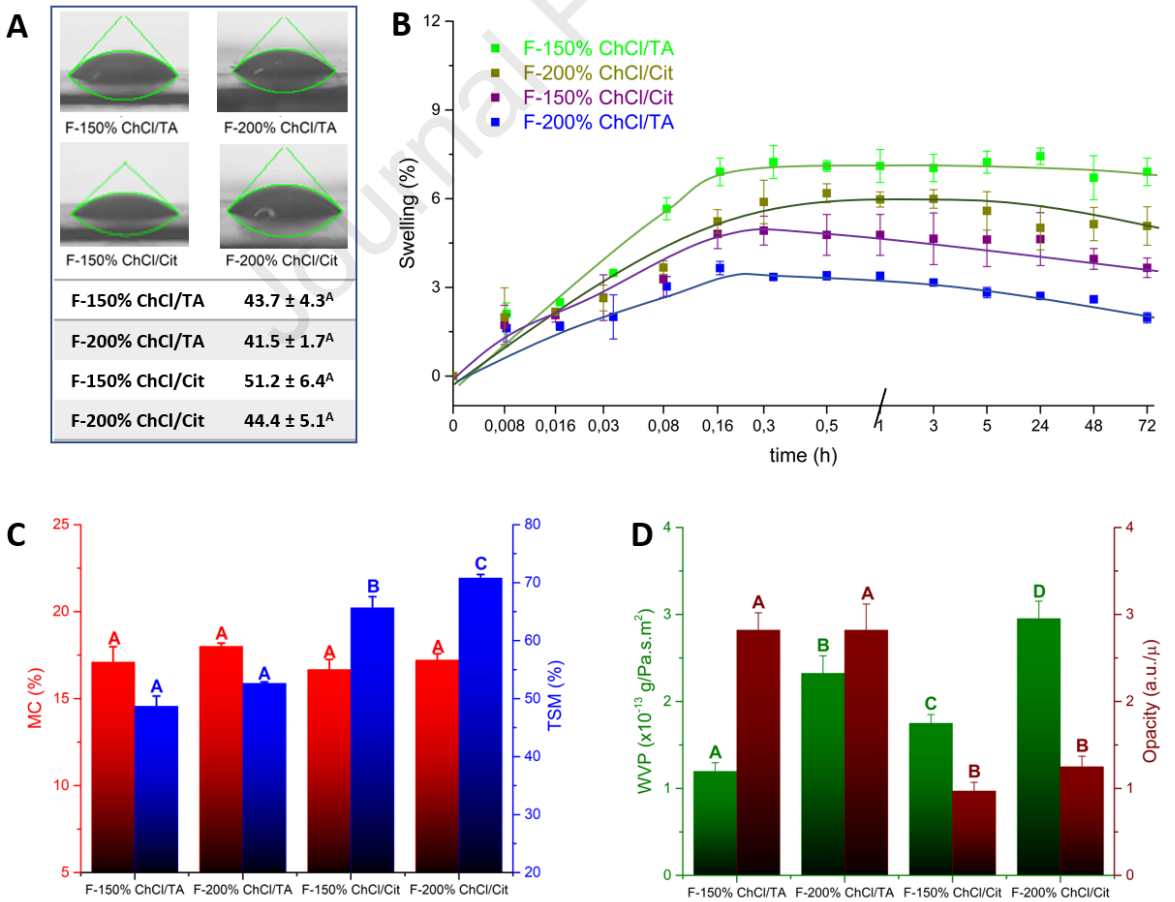

Fig. 6. Contact angle values for the different films (**A**). Water swelling behavior over time (**B**). MC

(red columns) and TSM (blue columns) values (**C**). WVP (green columns) and Opacity (brown columns) values (**D**). Two values in the same column followed by the same letter are not different (p≥0.05) according to the Tukey test.

3.7 Antioxidant and antibacterial activity

As displayed in Fig. 7A, all films have antioxidant activity. Nevertheless, films fabricated using ChCl/TA have the highest antioxidant activity than films with ChCl/Cit, independently of the NADES concentration employed. The highest activity of films with ChCl/TA compared to those with ChCl/Cit is attributed to the abundant pyrogallol groups of TA capable of donating electrons to the DPPH radical species, leading to a strong radical scavenging activity (Kim, Panda, Sadeghi, & Seo, 2023). These results show that incorporating ChCl/TA NADES with antioxidant activity into SPI films could enhance the functionality of packaging materials. It is important to note that standard SPI films containing 50 wt% glycerol do not possess antioxidant activity, as observed in the study conducted by Li *et al*. (Li et al., 2021). When expressing the antioxidant activity results as DPPH scavenging activity (%) (Eq. 7), the calculated values are over 80% for Ch/TA films, accounting for (82.1 ± 1.3) % and (82.3 ± 1.1) % for 150 and 200 wt% films. These results demonstrate excellent antioxidant capability, resulting in greater values than those reported by Yu *et al.* (Yu et al., 2023) for chitosan films with different NADES incorporated at 20 and 60 wt%.

Contamination by pathogenic microorganisms represents a significant challenge to food security. Antimicrobial packaging materials have emerged as an effective solution to safeguard food from such risks. Thus, the antibacterial activity of the as-prepared films against selected bacterial strains was investigated, as shown in Fig.

7B and Table 2. In all cases, the films prepared with ChCl/Cit exhibit high antibacterial activity, whereas films with ChCl/TA are only highly active against *S. aureus* (Gram-positive) and less or non-active against Gram-negative bacteria. Belhaoues *et al.* reported that TA showed good activity, especially against *S. aureus* and *E. faecalis*, suggesting a greater antibacterial effect on Gram-positive bacteria. The NADES mechanism is based on the damage of the cell membrane via hydrophobic-hydrophobic interactions, triggering the leakage of its critical constituents and causing bacteria death (Olatunde, Benjakul, Vongkamjan, & Amnuaikit, 2019). Specifically, TA works as an inhibitor of the NorA efflux pump, which is the main mechanism responsible for its antibacterial activity (Belhaoues, Amri, & Bensouilah, 2020). The Gram-positive bacteria have a thick layer of peptidoglycan on their wall, whereas the Gram-negative has a triple-layered cell wall (a cytoplasmic inner membrane, a thin peptidoglycan middle layer, and an outer layer membrane). The effectiveness of TA is explained by its ability to pass through the bacterial cell wall up to the internal membrane, interfering with the cell's metabolism and, therefore, causing its destruction. In Gram-positive bacteria, the activity of tannins is rapid, while in Gram-negative strains, it is slower due to the thicker membrane (Kaczmarek, 2020), as observed in Table 2, where the greatest inhibition diameters were against *S. aureus*.

The differences in the antibacterial activity between ChCl/Cit and ChCl/TA films could be due to the presence of carboxylic groups in Cit, which have been reported to be efficient in inducing bacteria death (Wei Zhang et al., 2022). Recently, Wen *et al*. prepared chitosan/gelatin films containing a eutectic mixture based on thymol and

649 octanoic acid (H. Wen et al., 2023). Comparing the inhibition diameter data of those
650 films, F-200% ChCl/Cit film presents a superior activity against *E. coli*. Additionally,
651 Zhang *et al.* prepared starch/chitosan/polyethyleneimine blend films crosslinked with
652 Cit, showing inhibition diameters of approximately 12 mm against *S. aureus* and *E.*
653 *coli* (J. Zhang, Han, Ben, Han, & Yin, 2023) compared to ≈ 30 mm for F-200%
654 ChCl/Cit.

655 Regarding the antibacterial activity of TA, Carnicero *et al.* developed hydrogels
656 combining poly(vinyl alcohol) and TA-coated cellulose nanocrystals, while Gulzar *et*
657 *al*. coated polylactic acid films with gelatin/chitosan, TA, and chitooligosaccharides
658 (Carnicero et al., 2022; Gulzar et al., 2022). Both materials exhibited smaller
659 inhibition diameters against *E. coli* and *S. aureus* than the SPI films containing
660 ChCl/TA. It is important to note that the inhibition diameter data of these works has
661 been normalized by the size of the discs used in the experiments for comparison
662 purposes. The significantly higher antimicrobial activity of films incorporating
663 ChCl/TA than similar materials is probably due to the liquid NADES allowing for high
664 loading of TA that otherwise cannot be reached with this bioactive compound in a
665 solid form. It is worth mentioning that the antibacterial activity of these films is purely
666 derived from the NADES incorporation, as SPI control films did not show
667 antibacterial activity against *S. aureus* and *E. coli* (Fig. S5), revealing the key role of
668 the eutectic mixtures in providing bioactive materials feature for food packaging
669 applications.

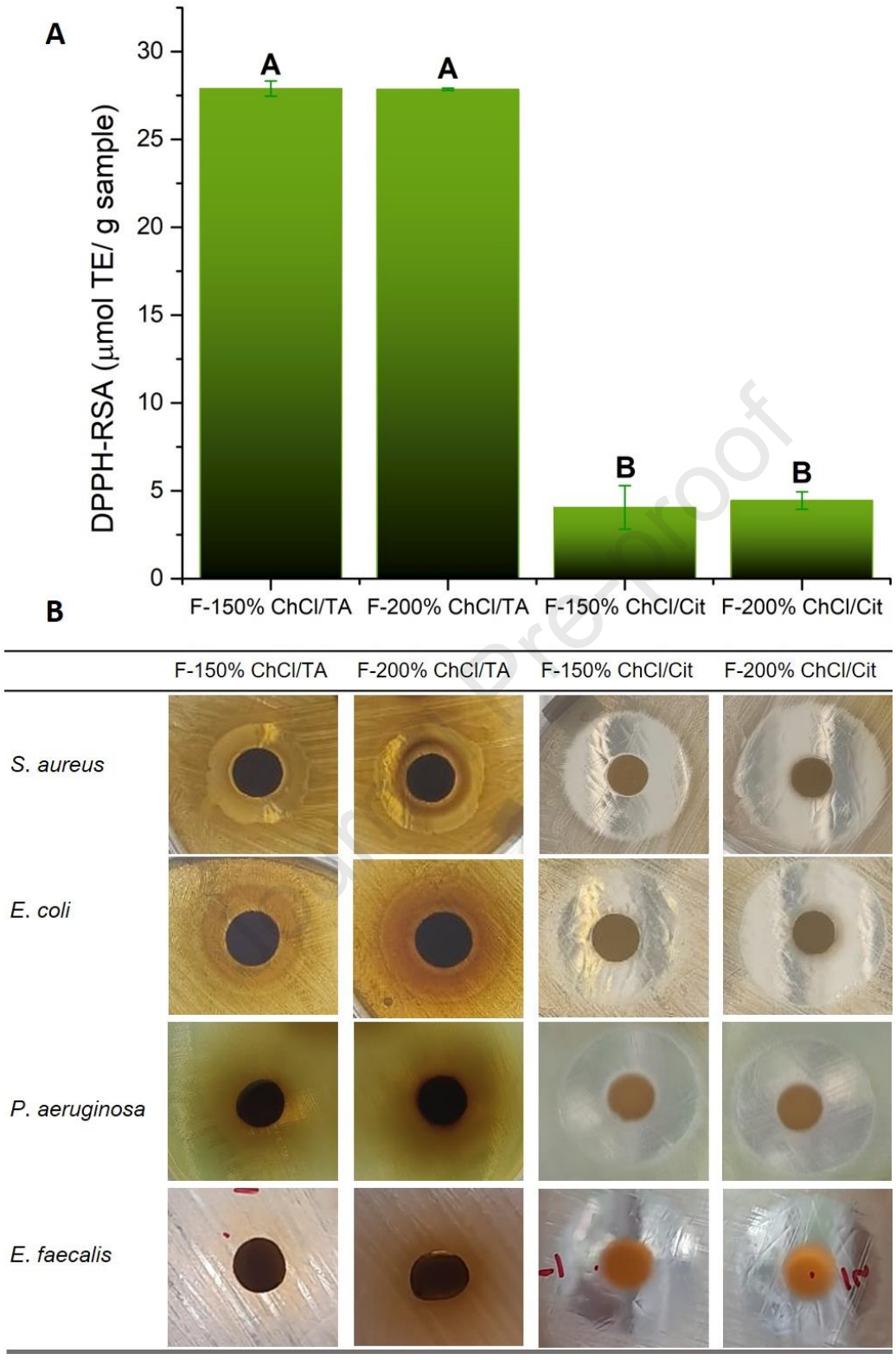

Fig. 7. (**A**) Antioxidant activities of the as-prepared films measured by DPPH assay. (**B**) Inhibition zones of films against *S. aureus, E. coli, P. aeruginosa,* and *E. faecalis determined by diffusion in agar method*. Two values in the same column followed by the same letter are not different (p≥0.05) according to the Tukey test.

675 **Table 2.** Diameter inhibition zones (mm). Films discs were 8 mm in diameter.

Strain	F-150% ChCl/TA	F-200% ChCl/TA	F-150% ChCl/Cit	F-200% ChCl/Cit
S. aureus	17.2 ± 0.4^{aA}	19.3 ± 0.6^{bA}	24.7 ± 0.4^{cA}	30.4 ± 0.6^{dA}
E. coli	8.5 ± 0.1^{aB}	9.1 ± 0.3^{bB}	21.1 ± 1.0^{cB}	27.4 ± 0.4^{cB}
P. aeruginosa	NA	NA	23.3 ± 0.9^{aA}	23.8 ± 0.5^{aC}
E. faecalis	8.7 ± 0.2^{aB}	10.1 ± 0.4^{bB}	22.9 ± 0.7^{cAB}	21.8 ± 0.5^{cD}

676 NA: no inhibitory activity.
677 Different lowercase superscripts within the same row indicate significant differences ($p < 0.05$).
678 Different uppercase superscripts within the same column indicate significant differences ($p < 0.05$).
679
680
681 *3.8 Antibacterial activity on chicken breast*
682
683
684 As displayed in Table 3, after 4 days, the chicken breast without film presented
685 markedly increased amounts of CFU with respect to t=0. In turn, the film of SPI with
686 50 wt% glycerol shows almost the same values of CFU as the control sample after
687 4 days indicating that it has no antimicrobial activity. Concerning to AMB, the films
688 with ChCl/TA demonstrate a considerable growth inhibition of colonies, and the films
689 with ChCl/Cit showed a better behavior, since a markedly increase in this
690 antimicrobial activity was evidenced. ENT is considered to be the indicator bacteria
691 for the microbiological quality of food and the hygiene status of a production process
692 (Mladenović et al., 2021). The count of ENT reveals that the films with ChCl/TA didn't
693 showed activity. This result is in agreement with the agar diffusion assay (section
694 3.7), since ENT are being a family of gram-negative bacteria with a thick membrane
695 that difficult the pass of TA towards the inside. For the films with ChCl/Cit, a
696 remarkable antimicrobial activity can be evidenced against the ENT family, as
697 expected according to the results shown in the previous section. The antimicrobial

activity of the films against *total coliforms,* which could indicate the possibility of fecal contamination of food (Silva, Rezende-Lago, Marchi, Messias, & Silva, 2023), follows the same trend that the result obtained against ENT since these bacteria are also gam-negative. Particularly, for the count of *E. coli*, all films with NADES present activity against this bacterial strain; however, no statistical differences are observed between the samples due to the low count of CFU given by the low initial value of CFU (control t=0). Finally, the presence of *S. aureus* was not detected for any sample.

Table 3. Microbiological results (log_{10} CFU/cm^2) of the chicken breast meat.

	AMB	*ENT*	*Total coliforms*	*E. coli*	*S. aureus*
Control t=0	0.17±0.01^{a}	0.12±0.01^{a}	0.11±0.01^{a}	0.06±0.01^{a}	<0.06±0.01^{a}
Control t=4 days	TNTC	0.18±0.02^{b}	0.17±0.02^{b}	0.1±0.01^{b}	<0.06±0.01^{a}
SPI 50 wt% glycerol	TNTC	0.18±0.01^{b}	0.16±0.02^{b}	0.09±0.01^{b}	<0.06±0.01^{a}
F-150% ChCl/TA	0.19±0.01^{a}	0.18±0.02^{b}	0.16±0.02^{b}	<0.05±0.01^{a}	<0.06±0.01^{a}
F-200% ChCl/TA	0.18±0.01^{a}	0.17±0.01^{b}	0.15±0.01^{b}	<0.05±0.01^{a}	<0.06±0.01^{a}
F-150% ChCl/Cit	0.14±0.01^{b}	0.06±0.01^{c}	<0.05±0.01^{a}	<0.05±0.01^{a}	<0.06±0.01^{a}
F-200% ChCl/Cit	0.14±0.01^{b}	0.09±0.01^{d}	0.07±0.01^{a}	<0.05±0.01^{a}	<0.06±0.01^{a}

TNTC = Too Numerous to Count
Two values in the same column followed by the same letter are not different (p≥0.05) according to the Tukey test.

4. Conclusions

This study presents a significant advancement in the synthesis of SPI films by incorporating NADES as bioactive agents, specifically tailored for enhancing food packaging applications. Despite the inherent hydrophilic nature of these films, their remarkable resistance to water swelling indicates the successful establishment of a robust crosslinked network between the NADES and SPI components. Notably, our investigation reveals that films containing ChCl/TA outperform those having ChCl/Cit in terms of tensile strength, underscoring the formation of a more resilient and compact molecular network within the former.

The introduction of ChCl/TA NADES produced a larger plasticizing effect on the films, compared to traditional glycerol-containing SPI films, which further expands their potential for flexible packaging solutions. Furthermore, the observed reduction in water vapor permeability underscores the dense interlinking between protein chains, accentuating the films' suitability for optimal food preservation.

Remarkably, ChCl/TA films exhibit a combination of high opacity and exceptional antioxidant activity, distinguishing them from ChCl/Cit films. Conversely, ChCl/Cit films display heightened antimicrobial efficacy. These findings collectively position these new films as promising candidates for safeguarding light-sensitive and pathogen-vulnerable food items.

Author statement

P.A.M designed and performed the research and wrote the manuscript; M.L.P and A.G designed the research, co-wrote the manuscript, and provided overall guidance.

Declaration of competing interest

The authors declare that they have no known competing financial interests or personal relationships that could have appeared to influence the work reported in this paper.

Acknowledgement

The authors acknowledge financial support from CONICET, FONCyT (PICT 2020-1955 and PICT-2019-4265) and SECyT-UNC (RES 411/18). P.A. Mercadal acknowledges the fellowship provided by CONICET.

References

Almeida, C. M. R., Magalhães, J. M. C. S., Souza, H. K. S., & Gonçalves, M. P. (2018). The role of choline chloride-based deep eutectic solvent and curcumin on chitosan films properties. *Food Hydrocolloids*, *81*, 456–466. https://doi.org/10.1016/j.foodhyd.2018.03.025

Alves, T. F. P., Teixeira, N., Vieira, J., Vicente, A. A., Mateus, N., de Freitas, V., & Souza, H. K. S. (2022). Sustainable chitosan packaging films: Green tea polyphenolic extraction strategies using deep eutectic solvents. *Journal of Cleaner Production*, *372*, 133589. https://doi.org/10.1016/j.jclepro.2022.133589

ASTM. (2002). Standard Test Method for Tensile Properties of Thin Plastic Sheeting (p. 9). https://doi.org/10.1520/D0882-02

760 ASTM. (2010). *Standard Test Methods for Water Vapor Transmission of Materials*.
761 https://doi.org/10.1520/E0096_E0096M-10

762 Azeredo, H. M. C., & Waldron, K. W. (2016). Crosslinking in polysaccharide and
763 protein films and coatings for food contact – A review. *Trends in Food Science*
764 *& Technology*, *52*, 109–122. https://doi.org/10.1016/j.tifs.2016.04.008

765 Ballesteros-Mártinez, L., Pérez-Cervera, C., & Andrade-Pizarro, R. (2020). Effect
766 of glycerol and sorbitol concentrations on mechanical, optical, and barrier
767 properties of sweet potato starch film. *NFS Journal*, *20*, 1–9.
768 https://doi.org/10.1016/j.nfs.2020.06.002

769 Belhaoues, S., Amri, S., & Bensouilah, M. (2020). Major phenolic compounds,
770 antioxidant and antibacterial activities of Anthemis praecox Link aerial parts.
771 *South African Journal of Botany*, *131*, 200–205.
772 https://doi.org/10.1016/j.sajb.2020.02.018

773 Carnicero, A., González, A., Dalosto, S. D., Passeggi, M. C. G., Minari, R. J.,
774 Alvarez Igarzabal, C. I., … Picchio, M. L. (2022). Ascidian-Inspired
775 Supramolecular Cellulose Nanocomposite Hydrogels with Antibacterial
776 Activity. *ACS Biomaterials Science & Engineering*, *8*(11), 5027–5037.
777 https://doi.org/10.1021/acsbiomaterials.2c00935

778 Casalini, S., & Giacinti Baschetti, M. (2023). The use of essential oils in chitosan or
779 cellulose-based materials for the production of active food packaging
780 solutions: a review. *Journal of the Science of Food and Agriculture*, *103*(3),
781 1021–1041. https://doi.org/10.1002/jsfa.11918

Chawla, R., Sivakumar, S., & Kaur, H. (2021). Antimicrobial edible films in food packaging: Current scenario and recent nanotechnological advancements- a review. *Carbohydrate Polymer Technologies and Applications*, *2*, 100024. https://doi.org/10.1016/j.carpta.2020.100024

Craveiro, R., Aroso, I., Flammia, V., Carvalho, T., Viciosa, M. T., Dionísio, M., … Paiva, A. (2016). Properties and thermal behavior of natural deep eutectic solvents. *Journal of Molecular Liquids*, *215*, 534–540. https://doi.org/10.1016/j.molliq.2016.01.038

Erdem, B. G., & Kaya, S. (2021). Production and application of freeze dried biocomposite coating powders from sunflower oil and soy protein or whey protein isolates. *Food Chemistry*, *339*, 127976. https://doi.org/10.1016/j.foodchem.2020.127976

Fang, X., Li, Y., Kua, Y. L., Chew, Z. L., Gan, S., Tan, K. W., … Lau, H. L. N. (2022). Insights on the potential of natural deep eutectic solvents (NADES) to fine-tune durian seed gum for use as edible food coating. *Food Hydrocolloids*, *132*, 107861. https://doi.org/10.1016/j.foodhyd.2022.107861

Florindo, C., Oliveira, F. S., Rebelo, L. P. N., Fernandes, A. M., & Marrucho, I. M. (2014). Insights into the Synthesis and Properties of Deep Eutectic Solvents Based on Cholinium Chloride and Carboxylic Acids. *ACS Sustainable Chemistry & Engineering*, *2*(10), 2416–2425. https://doi.org/10.1021/sc500439w

Florindo, Catarina, Oliveira, M. M., Branco, L. C., & Marrucho, I. M. (2017).

Carbohydrates-based deep eutectic solvents: Thermophysical properties and rice straw dissolution. *Journal of Molecular Liquids*, *247*, 441–447. https://doi.org/10.1016/j.molliq.2017.09.026

Galvis-Sánchez, A. C., Castro, M. C. R., Biernacki, K., Gonçalves, M. P., & Souza, H. K. S. (2018). Natural deep eutectic solvents as green plasticizers for chitosan thermoplastic production with controlled/desired mechanical and barrier properties. *Food Hydrocolloids*, *82*, 478–489. https://doi.org/10.1016/j.foodhyd.2018.04.026

Gennadios, A., Brandenburg, A. H., Weller, C. L., & Testin, R. F. (1993). Effect of pH on properties of wheat gluten and soy protein isolate films. *Journal of Agricultural and Food Chemistry*, *41*(11), 1835–1839. https://doi.org/10.1021/jf00035a006

González, A., Barrera, G. N., Galimberti, P. I., Ribotta, P. D., & Alvarez, C. I. (2019). Development of edible films prepared by soy protein and the galactomannan fraction extracted from Gleditsia triacanthos (Fabaceae) seed. *Food Hydrocolloids*, *97*(February), 105227. https://doi.org/10.1016/j.foodhyd.2019.105227

González, A., Gastelú, G., Barrera, G. N., Ribotta, P. D., & Álvarez Igarzabal, C. I. (2019). Preparation and characterization of soy protein films reinforced with cellulose nanofibers obtained from soybean by-products. *Food Hydrocolloids*, *89*, 758–764. https://doi.org/10.1016/j.foodhyd.2018.11.051

Grala, D., Biernacki, K., Freire, C., Kuźniarska-Biernacka, I., Souza, H. K. S., &

826 Gonçalves, M. P. (2022). Effect of natural deep eutectic solvent and chitosan
827 nanoparticles on physicochemical properties of locust bean gum films. *Food*
828 *Hydrocolloids*, *126*, 107460. https://doi.org/10.1016/j.foodhyd.2021.107460

829 Guerrero, P., & de la Caba, K. (2010). Thermal and mechanical properties of soy
830 protein films processed at different pH by compression. *Journal of Food*
831 *Engineering*, *100*(2), 261–269. https://doi.org/10.1016/j.jfoodeng.2010.04.008

832 Guilbert, S., Gontard, N., & Cuq, B. (1995). Technology and applications of edible
833 protective films. *Packaging Technology and Science*, *8*(6), 339–346.
834 https://doi.org/10.1002/pts.2770080607

835 Gulzar, S., Tagrida, M., Nilsuwan, K., Prodpran, T., & Benjakul, S. (2022).
836 Electrospinning of gelatin/chitosan nanofibers incorporated with tannic acid
837 and chitooligosaccharides on polylactic acid film: Characteristics and
838 bioactivities. *Food Hydrocolloids*, *133*, 107916.
839 https://doi.org/10.1016/j.foodhyd.2022.107916

840 Hoyos-Merlano, N. T., Borroni, V., Rodriguez-Batiller, M. J., Candal, R. J., &
841 Herrera, M. L. (2022). Nanoreinforcement as a strategy to improve physical
842 properties of biodegradable composite films based on biopolymers. *Food*
843 *Research International*, *162*, 112178.
844 https://doi.org/10.1016/j.foodres.2022.112178

845 Hu, X. Z., Cheng, Y. Q., Fan, J. F., Lu, Z. H., Yamaki, K., & Li, L. Te. (2009).
846 Effects of Drying Method on Physicochemical and Functional Properties of
847 Soy Protein Isolates. *Journal of Food Processing and Preservation*, *34*(3),

520–540. https://doi.org/10.1111/j.1745-4549.2008.00357.x

Jakubowska, E., Gierszewska, M., Nowaczyk, J., & Olewnik-Kruszkowska, E. (2020). Physicochemical and storage properties of chitosan-based films plasticized with deep eutectic solvent. *Food Hydrocolloids*, *108*(April), 106007. https://doi.org/10.1016/j.foodhyd.2020.106007

Kaczmarek, B. (2020). Tannic Acid with Antiviral and Antibacterial Activity as A Promising Component of Biomaterials—A Minireview. *Materials*, *13*(14), 3224. https://doi.org/10.3390/ma13143224

Kang, H., Wang, Z., Zhang, W., Li, J., & Zhang, S. (2016). Physico-chemical properties improvement of soy protein isolate films through caffeic acid incorporation and tri-functional aziridine hybridization. *Food Hydrocolloids*, *61*, 923–932. https://doi.org/10.1016/j.foodhyd.2016.07.009

Kim, H., Panda, P. K., Sadeghi, K., & Seo, J. (2023). Poly (vinyl alcohol)/hydrothermally treated tannic acid composite films as sustainable antioxidant and barrier packaging materials. *Progress in Organic Coatings*, *174*(July 2022). https://doi.org/10.1016/j.porgcoat.2022.107305

Kovačič, S., Žagar, E., & Slugovc, C. (2019). Strength versus toughness of emulsion templated Poly(Dicyclopentadiene) foams. *Polymer*, *169*, 58–65. https://doi.org/10.1016/j.polymer.2019.02.045

Lee, S. J., Gwak, M. A., Chathuranga, K., Lee, J. S., Koo, J., & Park, W. H. (2023). Multifunctional chitosan/tannic acid composite films with improved anti-UV, antioxidant, and antimicrobial properties for active food packaging. *Food*

Hydrocolloids, *136*, 108249. https://doi.org/10.1016/j.foodhyd.2022.108249

Li, T., Xia, N., Xu, L., Zhang, H., Zhang, H., Chi, Y., … Li, H. (2021). Preparation, characterization and application of SPI-based blend film with antioxidant activity. *Food Packaging and Shelf Life*, *27*, 100614. https://doi.org/10.1016/j.fpsl.2020.100614

Liu, P., Xu, H., Zhao, Y., & Yang, Y. (2017). Rheological properties of soy protein isolate solution for fibers and films. *Food Hydrocolloids*, *64*, 149–156. https://doi.org/10.1016/j.foodhyd.2016.11.001

Liu, W., Kang, S., Zhang, Q., Chen, S., Yang, Q., & Yan, B. (2023). Self-assembly fabrication of chitosan-tannic acid/MXene composite film with excellent antibacterial and antioxidant properties for fruit preservation. *Food Chemistry*, *410*(December 2022), 135405. https://doi.org/10.1016/j.foodchem.2023.135405

Manzoor, A., Yousuf, B., Pandith, J. A., & Ahmad, S. (2023). Plant-derived active substances incorporated as antioxidant, antibacterial or antifungal components in coatings/films for food packaging applications. *Food Bioscience*, *53*, 102717. https://doi.org/10.1016/j.fbio.2023.102717

Mercadal, P. A., Romero, M. R., Montesinos, M. del M., Real, J. P., Picchio, M. L., & González, A. (2023). Natural, Biocompatible, and 3D-Printable Gelatin Eutectogels Reinforced with Tannic Acid-Coated Cellulose Nanocrystals for Sensitive Strain Sensors. *ACS Applied Electronic Materials*. https://doi.org/10.1021/acsaelm.3c00075

892 Mercadal, P., Romero, M., Montesinos, M. del M., Real, J. P., Picchio, M., &
893 Gonzalez, A. (2023). Natural, Biocompatible, and 3D-Printable Gelatin
894 Eutectogels Reinforced with Tannic Acid Coated Cellulose Nanocrystals for
895 Sensitive Strain Sensors. *ACS Applied Electronic Materials Aceptado En*
896 *Prensa. 2023*.

897 Mladenović, K. G., Grujović, M. Ž., Kiš, M., Furmeg, S., Tkalec, V. J., Stefanović,
898 O. D., & Kocić-Tanackov, S. D. (2021). Enterobacteriaceae in food safety with
899 an emphasis on raw milk and meat. *Applied Microbiology and Biotechnology*,
900 *105*(23), 8615–8627. https://doi.org/10.1007/s00253-021-11655-7

901 Olatunde, O. O., Benjakul, S., Vongkamjan, K., & Amnuaikit, T. (2019). Liposomal
902 Encapsulated Ethanolic Coconut Husk Extract: Antioxidant and Antibacterial
903 Properties. *Journal of Food Science*, *84*(12), 3664–3673.
904 https://doi.org/10.1111/1750-3841.14853

905 Oliveira Filho, J. G. de, Rodrigues, J. M., Valadares, A. C. F., Almeida, A. B. de,
906 Lima, T. M. de, Takeuchi, K. P., … Egea, M. B. (2019). Active food packaging:
907 Alginate films with cottonseed protein hydrolysates. *Food Hydrocolloids*, *92*,
908 267–275. https://doi.org/10.1016/j.foodhyd.2019.01.052

909 Paiva, A., Craveiro, R., Aroso, I., Martins, M., Reis, R. L., & Duarte, A. R. C.
910 (2014). Natural Deep Eutectic Solvents – Solvents for the 21st Century. *ACS*
911 *Sustainable Chemistry & Engineering*, *2*(5), 1063–1071.
912 https://doi.org/10.1021/sc500096j

913 Picchio, M. L., Linck, Y. G., Monti, G. A., Gugliotta, L. M., Minari, R. J., & Alvarez

Igarzabal, C. I. (2018). Casein films crosslinked by tannic acid for food packaging applications. *Food Hydrocolloids*, *84*(April), 424–434. https://doi.org/10.1016/j.foodhyd.2018.06.028

Picchio, M. L., Minudri, D., Mantione, D., Criado-Gonzalez, M., Guzmán-González, G., Schmarsow, R., … Mecerreyes, D. (2022). Natural Deep Eutectic Solvents Based on Choline Chloride and Phenolic Compounds as Efficient Bioadhesives and Corrosion Protectors. *ACS Sustainable Chemistry and Engineering*, *10*(25), 8135–8142. https://doi.org/10.1021/acssuschemeng.2c01976

Płotka-Wasylka, J., de la Guardia, M., Andruch, V., & Vilková, M. (2020). Deep eutectic solvents vs ionic liquids: Similarities and differences. *Microchemical Journal*, *159*, 105539. https://doi.org/10.1016/j.microc.2020.105539

Pontillo, A. R. N., Koutsoukos, S., Welton, T., & Detsi, A. (2021). Investigation of the influence of natural deep eutectic solvents (NaDES) in the properties of chitosan-stabilised films. *Materials Advances*, *2*(12), 3954–3964. https://doi.org/10.1039/D0MA01008A

Rhim, J.-W., Gennadios, A., Weller, C. L., Carole Cezeirat, & Hanna, M. A. (1998). Soy protein isolate–dialdehyde starch films. *Industrial Crops and Products*, *8*(3), 195–203. https://doi.org/10.1016/S0926-6690(98)00003-X

Romero, M. R., Wolfel, A., & Igarzabal, C. I. A. (2016). Smart valve: Polymer actuator to moisture soil control. *Sensors and Actuators, B: Chemical*, *234*, 53–62. https://doi.org/10.1016/j.snb.2016.04.104

Salfinger, Y., & Tortorello, M. Lou (Eds.). (2015). *Compendium of Methods for the Microbiological Examination of Foods*. American Public Health Association. https://doi.org/10.2105/MBEF.0222

Salihu, R., Abd Razak, S. I., Ahmad Zawawi, N., Rafiq Abdul Kadir, M., Izzah Ismail, N., Jusoh, N., … Hasraf Mat Nayan, N. (2021). Citric acid: A green cross-linker of biomaterials for biomedical applications. *European Polymer Journal*, *146*, 110271. https://doi.org/10.1016/j.eurpolymj.2021.110271

Schmidt, V., Giacomelli, C., & Soldi, V. (2005). Thermal stability of films formed by soy protein isolate–sodium dodecyl sulfate. *Polymer Degradation and Stability*, *87*(1), 25–31. https://doi.org/10.1016/j.polymdegradstab.2004.07.003

Shafie, M. H., Yusof, R., & Gan, C.-Y. (2019). Synthesis of citric acid monohydrate-choline chloride based deep eutectic solvents (DES) and characterization of their physicochemical properties. *Journal of Molecular Liquids*, *288*, 111081. https://doi.org/10.1016/j.molliq.2019.111081

Silva, I. F., Rezende-Lago, N. C. M. de, Marchi, P. G. F. de, Messias, C. T., & Silva, L. A. (2023). Microbiological Quality of Food. In *COLLECTION OF INTERNATIONAL TOPICS IN HEALTH SCIENCE- V1* (pp. 1501–1518). Seven Editora. https://doi.org/10.56238/colleinternhealthscienv1-120

Silva, L. P., Martins, M. A. R., Conceição, J. H. F., Pinho, S. P., & Coutinho, J. A. P. (2020). Eutectic Mixtures Based on Polyalcohols as Sustainable Solvents: Screening and Characterization. *ACS Sustainable Chemistry and Engineering*, *8*(40), 15317–15326. https://doi.org/10.1021/acssuschemeng.0c05518

Smirnov, M. A., Nikolaeva, A. L., Bobrova, N. V., Vorobiov, V. K., Smirnov, A. V., Lahderanta, E., & Sokolova, M. P. (2021). Self-healing films based on chitosan containing citric acid/choline chloride deep eutectic solvent. *Polymer Testing*, *97*, 107156. https://doi.org/10.1016/j.polymertesting.2021.107156

Sousa, A. S. B. de, Lima, R. P., Silva, M. C. A. da, Moreira, D. das N., Pintado, M. M. E., & Silva, S. de M. (2022). Natural deep eutectic solvent of choline chloride with oxalic or ascorbic acids as efficient starch-based film plasticizers. *Polymer*, *259*(May), 125314. https://doi.org/10.1016/j.polymer.2022.125314

Strauss, G., & Gibson, S. M. (2004). Plant phenolics as cross-linkers of gelatin gels and gelatin-based coacervates for use as food ingredients. *Food Hydrocolloids*, *18*(1), 81–89. https://doi.org/10.1016/S0268-005X(03)00045-6

Tang, C.-H., Choi, S.-M., & Ma, C.-Y. (2007). Study of thermal properties and heat-induced denaturation and aggregation of soy proteins by modulated differential scanning calorimetry. *International Journal of Biological Macromolecules*, *40*(2), 96–104. https://doi.org/10.1016/j.ijbiomac.2006.06.013

Tao, R., Sedman, J., & Ismail, A. (2022). Characterization and in vitro antimicrobial study of soy protein isolate films incorporating carvacrol. *Food Hydrocolloids*, *122*, 107091. https://doi.org/10.1016/j.foodhyd.2021.107091

Tian, Y., Sun, D.-W., Xu, L., Fan, T.-H., & Zhu, Z. (2022). Bio-inspired eutectogels enabled by binary natural deep eutectic solvents (NADESs): Interfacial anti-frosting, freezing-tolerance, and mechanisms. *Food Hydrocolloids*, *128*, 107568. https://doi.org/10.1016/j.foodhyd.2022.107568

Vieira, I. R. S., de Carvalho, A. P. A. de, & Conte-Junior, C. A. (2022). Recent advances in biobased and biodegradable polymer nanocomposites, nanoparticles, and natural antioxidants for antibacterial and antioxidant food packaging applications. *Comprehensive Reviews in Food Science and Food Safety*, *21*(4), 3673–3716. https://doi.org/10.1111/1541-4337.12990

Wang, J., Zhang, S., Ma, Z., & Yan, L. (2021). Deep eutectic solvents eutectogels: progress and challenges. *Green Chemical Engineering*, *2*(4), 359–367. https://doi.org/10.1016/j.gce.2021.06.001

Wei, L., Zhang, W., Yang, J., Pan, Y., Chen, H., & Zhang, Z. (2023). The application of deep eutectic solvents systems based on choline chloride in the preparation of biodegradable food packaging films. *Trends in Food Science and Technology*, *139*(July), 104124. https://doi.org/10.1016/j.tifs.2023.104124

Wen, H., Tang, D., Lin, Y., Zou, J., Liu, Z., Zhou, P., & Wang, X. (2023). Enhancement of water barrier and antimicrobial properties of chitosan/gelatin films by hydrophobic deep eutectic solvent. *Carbohydrate Polymers*, *303*, 120435. https://doi.org/10.1016/j.carbpol.2022.120435

Wen, L., Liang, Y., Lin, Z., Xie, D., Zheng, Z., Xu, C., & Lin, B. (2021). Design of multifunctional food packaging films based on carboxymethyl chitosan/polyvinyl alcohol crosslinked network by using citric acid as crosslinker. *Polymer*, *230*, 124048. https://doi.org/10.1016/j.polymer.2021.124048

Yu, J., Xu, S., Goksen, G., Yi, C., & Shao, P. (2023). Chitosan films plasticized with

choline-based deep eutectic solvents: UV shielding, antioxidant, and antibacterial properties. *Food Hydrocolloids*, *135*(April 2022), 108196. https://doi.org/10.1016/j.foodhyd.2022.108196

Zdanowicz, M., Spychaj, T., & Mąka, H. (2016). Imidazole-based deep eutectic solvents for starch dissolution and plasticization. *Carbohydrate Polymers*, *140*, 416–423. https://doi.org/10.1016/j.carbpol.2015.12.036

Zhang, J., Han, Y., Ben, Z., Han, T., & Yin, P. (2023). Effect of branched polyethyleneimine and citric acid on the structural, physical and antibacterial properties of corn starch/chitosan films. *International Journal of Biological Macromolecules*, *231*, 123186. https://doi.org/10.1016/j.ijbiomac.2023.123186

Zhang, Wanli, Roy, S., Assadpour, E., Cong, X., & Jafari, S. M. (2023). Cross-linked biopolymeric films by citric acid for food packaging and preservation. *Advances in Colloid and Interface Science*, *314*, 102886. https://doi.org/10.1016/j.cis.2023.102886

Zhang, Wanli, Roy, S., Ezati, P., Yang, D.-P., & Rhim, J.-W. (2023). Tannic acid: A green crosslinker for biopolymer-based food packaging films. *Trends in Food Science & Technology*, *136*, 11–23. https://doi.org/10.1016/j.tifs.2023.04.004

Zhang, Wei, Shen, J., Gao, P., Jiang, Q., & Xia, W. (2022). Sustainable chitosan films containing a betaine-based deep eutectic solvent and lignin: Physicochemical, antioxidant, and antimicrobial properties. *Food Hydrocolloids*, *129*, 107656. https://doi.org/10.1016/j.foodhyd.2022.107656

Zhao, P., Wang, J., Yan, X., Cai, Z., Fu, L., Gu, Q., … Fu, Y. (2022). Functional

chitosan/zein films with Rosa roxburghii Tratt leaves extracts prepared by natural deep eutectic solvents. *Food Packaging and Shelf Life*, *34*, 101001. https://doi.org/10.1016/j.fpsl.2022.101001

TOC

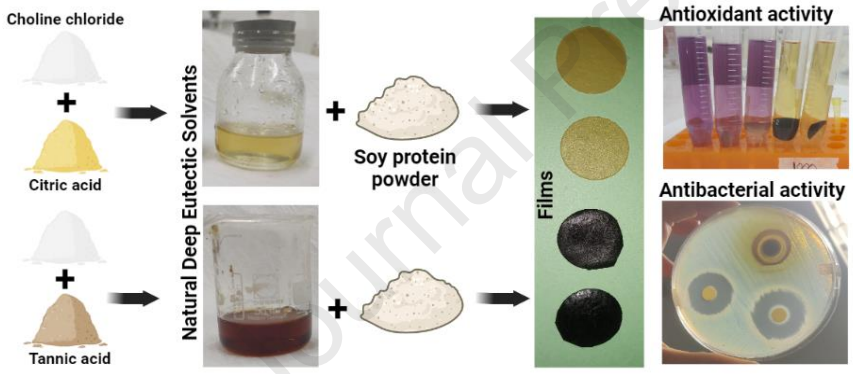

Highlights

- Soy protein films were prepared with tannic acid and citric acid based NADES.
- Liquid NADES allows for high TA and Cit loading without phase separation in the films.
- NADES-containing films showed lower water vapor permeability values.
- Films with ChCl/TA exhibited high light barrier properties and antioxidant activity.
- Films with ChCl/Cit demonstrated superior antimicrobial activity.

Author Statement

Pablo A. Mercadal: Investigation; Formal Analysis, Writing - Original Draft; Visualization.

Matias L. Picchio: Conceptualization, Formal analysis; Writing - Review & Editing, Supervision; Funding acquisition.

Agustín González: Conceptualization, Methodology, Investigation, Formal analysis, Writing - Original Draft; Writing - Review & Editing, Supervision; Project administration, Funding acquisition.

Declaration of interests

☒ The authors declare that they have no known competing financial interests or personal relationships that could have appeared to influence the work reported in this paper.

☐The authors declare the following financial interests/personal relationships which may be considered as potential competing interests: